GEOSPATIAL IDENTIFICATION OF SOIL EROSION HOTSPOTS EXACERBATING THE CATASTROPHIC FLASH FLOOD IN BALI, INDONESIA

Ni Made TRIGUNASIH [1], ***Moh SAIFULLOH*** [2,3*], ***I Nyoman SUNARTA*** [4], ***Ida Bagus Putu BHAYUNAGIRI*** [1] ***& Zulkarnain ZULKARNAIN*** [5]

DOI: 10.21163/GT_2026.211.09

ABSTRACT

The catastrophic flash flood that struck the Biluk Poh Watershed in Bali on October 16, 2022, was a complex disaster. While triggered by extreme rainfall, its catastrophic scale was critically exacerbated by landscape-level factors, particularly massive sediment mobilization. This study investigates the spatial contribution of soil erosion to the flood's severity by quantifying its extent and intensity using the Universal Soil Loss Equation (USLE). The analysis integrates CHIRPS rainfall data, ALOS PALSAR DEM, vegetation indices from Sentinel-2, and field-based measurements of soil structure, texture, and organic matter. High-resolution erosion modelling (10 m) revealed soil loss ranging from 0 to 4664.78 t ha^{-1} yr^{-1}, with a watershed average of 168.03 t ha^{-1} yr^{-1}. The results show a landscape of stark contrasts: while 39.30% of the area experiences only Slight erosion (0–15 t ha^{-1} yr^{-1}), a combined 55.97% suffers from Moderate (18.56%), Heavy (29.42%), and Very Heavy (7.99%) erosion. Erosion was most severe in the Penyaringan and Yeh Embang Kauh villages. These findings demonstrate that uncontrolled erosion from these specific hotspots, which are concentrated upstream and along steep river corridors, functioned as the key exacerbating factor. They supplied the massive sediment loads that blocked the main river channel, catastrophically worsening the flood event triggered by high rainfall. This study provides the first high-resolution erosion assessment for the Biluk Poh Watershed, offering critical evidence for targeted mitigation. The urgency of these findings is underscored by the catastrophic September 2025 Bali floods, which demonstrated that the sediment-driven mechanisms modeled in this study are a primary, escalating, and regional-scale threat.

Keywords: *Erosion modeling; Bali flooding; Flash flood; Disaster risk reduction; Watershed management.*

1. INTRODUCTION

Soil erosion is one of the most widespread and critical forms of land degradation, particularly in tropical regions where high rainfall intensity and complex topography prevail (Ao et al., 2025; Kardhana et al., 2024; Mahmood et al., 2024). The detachment and transport of topsoil by surface runoff not only reduce land productivity but also contribute to sedimentation in rivers, reservoirs, and irrigation systems, impairing hydrological function and increasing the risk of downstream flooding (Rashmi et al., 2022). These impacts are frequently intensified by unsustainable land management practices, including deforestation and insufficient conservation infrastructure (Hirabayashi et al., 2021). While flash floods are typically associated with short-duration, high-intensity rainfall, their severity is often exacerbated by pre-existing landscape vulnerabilities such as soil erosion, sediment accumulation, and reduced river channel capacity (Chen et al., 2024; Singh & Kansal, 2024).

---

[1]*Soil Sciences and Environment Laboratory, Faculty of Agriculture, Udayana University, Denpasar, Indonesia. trigunasih@unud.ac.id (NMT), bhayunagiri@unud.ac.id (IBPB).*

[2]*Spatial Data Infrastructure Development Centre (PPIDS) Udayana University, Denpasar, Indonesia.*

[3*]*Marine Sciences Study Program, Faculty of Marine Sciences and Fisheries, Udayana University-Badung, Indonesia. Corresponding author: m.saifulloh@unud.ac.id (MS).*

[4]*Doctoral Program of Tourism, Faculty of Tourism, Udayana University, Denpasar, Indonesia. nyoman_sunarta@unud.ac.id (INS).*

[5]*Agroecotechnology Study Program, Faculty of Agriculture, Mulawarman University, Samarinda, East Kalimantan, Indonesia. zulkarnain@faperta.unmul.ac.id (ZZ).*

Erosion accelerates surface runoff, mobilizes sediment, and contributes to channel clogging, creating hazardous conditions during storm events (Wink Junior et al., 2024). This sediment influx promotes channel aggradation, which reduces the hydraulic conveyance capacity of the river. Consequently, channel overbank flow can occur at lower discharge volumes, amplifying the flood's magnitude and spatial extent (Addy & Wilkinson, 2021; Ahrendt et al., 2022). Despite this direct link, soil erosion is rarely included as a central parameter in flood risk studies, which often emphasize rainfall variability or land-use change (Wu et al., 2023; Zhang et al., 2024). This oversight can limit the understanding of flood generation processes, particularly in watersheds susceptible to high sediment yields.

Flash flood risk is primarily driven by the temporal variability of high-intensity precipitation. However, the impacts of these rainfall events are spatially heterogeneous at the watershed scale. This variability is shaped by landscape-level exacerbating factors, including land-use change and the inherent susceptibility of the landscape to soil erosion, which influences runoff generation, sediment transport, and other key physical processes (Abu El-Magd et al., 2021; Bauer et al., 2019). This landscape vulnerability to erosion is captured by the components of the Universal Soil Loss Equation (USLE) model: soil vulnerability (K factor), topographic vulnerability (LS factor), the impact of land use practices (P factor), and the protective role of vegetation cover (C factor). Global research has increasingly demonstrated how soil erosion acts as this critical exacerbating factor, rather than a direct driver, in flash flood risk. For example, in Makkah City, high erosion was concentrated in 11% of the watershed, determining where flood risk was highest (Othman et al., 2023). In China's Wuding River Basin, erosion hotspots at river confluences were identified as the source of sedimentation that triggered severe flash floods (Lai et al., 2024). Similarly, long-term analysis in North Africa linked climate extremes and urban development to a 24.14% increase in erosion-driven exposure of human populations (Salhi et al., 2024).

The USLE and its revised form (RUSLE) are two examples of empirical approaches that have become more popular for modeling soil erosion around the world (Lamane et al., 2025; Prasad et al., 2024; Taloor et al., 2025), especially when combined with Geographic Information Systems (GIS) and satellite-based remote sensing. Many studies in Asia, Africa, and Europe have used these models successfully to measure yearly soil loss at the watershed and regional levels using open-access geospatial datasets, especially from sensors like Landsat and Sentinel-2 (Dou et al., 2022; Dzwairo et al., 2025; Milazzo et al., 2023; Panagos et al., 2024). But a lot of these apps tend to make assumptions about important factors like the soil erodibility factor (K) based on old databases or broad soil classification maps, which might not show how complicated the land is in previous case studies (Soniari et al., 2024). Also, the Normalized Difference Vegetation Index (NDVI) is often the only source of vegetation cover, even though it does not work well in areas with mixed or sparse vegetation (Gwapedza et al., 2021; Okacha & Salhi, 2024). This leads to assessments that are too simple and may miss important micro-scale erosion processes, especially in tropical landscapes that change quickly.

This study makes a new contribution by combining high-resolution remote sensing with detailed field-based soil observations to make erosion models more accurate. The K factor is based on ground-measured soil texture, organic matter, and structural conditions. This makes it possible to get realistic estimates of how easily the soil can be eroded that are specific to the geomorphological and geological diversity of the Biluk Poh Watershed. We also use the Perpendicular Vegetation Index (PVI) and the Normalized Difference Soil Vegetation Index (NDSVI) in addition to NDVI. These are better at picking up on changes in vegetation and canopy density (Adnyana et al., 2024; Adnyana et al., 2025). These changes make it much easier to guess the C factor. Our dataset is cheaper and more scalable than previous studies in Bali Province, which mostly used traditional field-based erosion assessments with limited spatial coverage (Soniari et al., 2024; Trigunasih et al., 2018; Trigunasih & Saifulloh, 2023). It also helps with early-warning and risk reduction strategies in tropical watersheds that are prone to erosion. In Indonesia, many watershed studies focus on land-use dynamics, with limited exploration of soil erosion as a key hydrological variable. For instance, research in Aceh Jaya's Teunom Watershed identified that 68% of the area was exposed to moderate to high flood risk due to

declining forest and agricultural cover (Sugianto et al., 2022). Similarly, the Garang Watershed in Semarang experienced spatial degradation driven by overlapping management and weak planning enforcement (Sejati et al., 2024). Although these studies reveal the importance of land use, few have incorporated detailed erosion assessments or quantified sedimentation hazards directly (Merten et al., 2020; Wardhani et al., 2022). This oversight is especially problematic in regions like Bali, where steep volcanic slopes, intense rainfall, and degraded soils contribute to heightened erosion susceptibility.

On 16 October 2022, the Biluk Poh Watershed in Jembrana Regency, Bali, experienced a flash flood that inflicted widespread damage to settlement, roads, and bridges. While the intense rainfall is documented as the temporal trigger, the role of geomorphic and soil-related factors as key exacerbating factors remains unexplored. This study addresses that critical knowledge gap. The primary objective is to provide a rapid geospatial identification of soil erosion hotspots, framing them as the principal landscape-level factors that amplified the flood's catastrophic severity by contributing massive volumes of sediment to the river system. To achieve this, the novelty of our research lies in its high-resolution (10 m), field-calibrated methodology. This approach is specifically designed to overcome the limitations of broader regional studies that rely on generalized soil databases. Our methodology integrates ground-measured soil parameters (texture, organic matter, and structure) to derive a locally-specific K factor and utilizes advanced vegetation indices (PVI and NDSVI) from Sentinel-2 for a more accurate C factor. This field calibration is essential for accurately capturing the high spatial variability of tropical volcanic landscapes like the Biluk Poh Watershed. This robust USLE model allows us to quantify erosion rates by integrating the rainfall driver (R factor) with the spatial landscape variables that control susceptibility (K, LS, C, and P). This study then conceptually links the resulting erosion hotspot map to the observed flood impacts through a visual analysis of high-resolution Unmanned Aerial Vehicle (UAV) imagery captured post-event. This combined analysis provides a critical, spatially-explicit evidence base for strategic soil conservation planning aimed at reducing future sedimentation-driven flood risks in this vulnerable tropical watershed.

2. STUDY AREA

This study was conducted in the Biluk Poh Watershed, located in Jembrana Regency, Bali Province, Indonesia. The watershed spans an area of 9,109.67 ha and is geographically situated between latitudes 8°12′30″S and 8°22′30″S and longitudes 114°00′00″E and 114°47′30″E (**Fig. 1**).

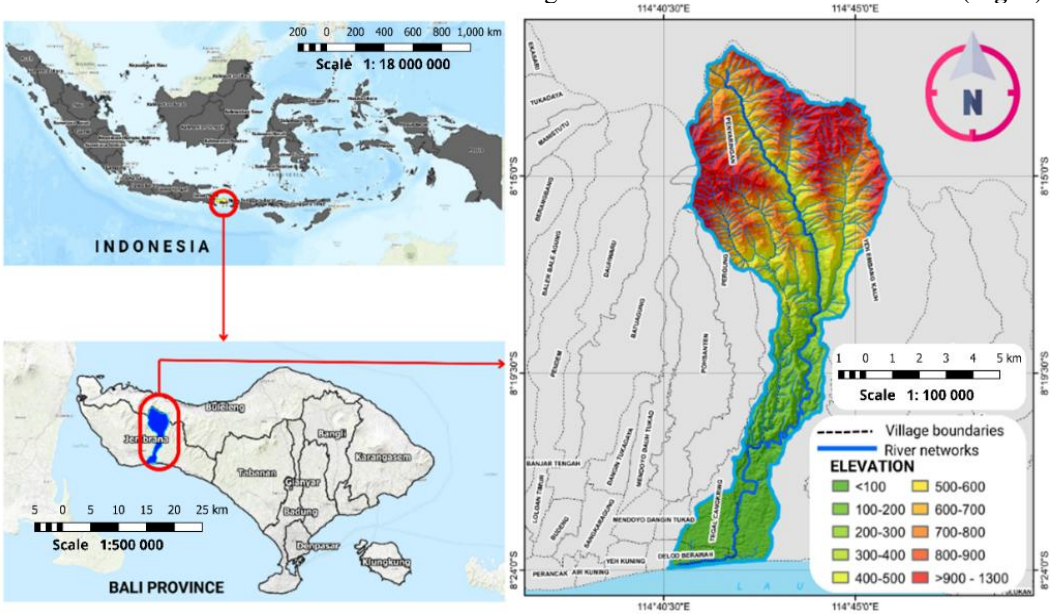

Fig. 1. Geographical location of the catastrophic flash flood event in Bali, Indonesia.

Based on the geomorphological map produced by Suyarto and Wiyanti (2023), the landscape is predominantly volcanic. Mid-slope volcanic terrain accounts for 69.06% of the total area, while additional volcanic landforms include upper volcanic slopes (8.98%), lower volcanic slopes (8.91%), and volcanic footslopes (2.18%). In the downstream section of the watershed, coastal landforms are present, consisting of fluviomarine plains (9.83%) and alluvial plains (2.03%).

Elevation across the watershed ranges from 0 to 1,318 meters above sea level (masl). The majority of the area (67.15%) lies above 500 masl, followed by 16.31% within the 0–100 masl range, and 12.54% between 100–500 masl. This geomorphological heterogeneity, encompassing both volcanic and coastal landforms, contributes significantly to variations in surface runoff, sediment transport, and erosion potential. These conditions establish the Biluk Poh Watershed as a highly suitable site for detailed spatial erosion analysis and for understanding upstream-to-downstream sediment dynamics.

3. METHOD

3.1. Data Sources

This study employed an integrated approach combining remote sensing datasets and field-based soil data to quantify erosion hazards in the watershed. All datasets represent conditions for the year 2022, corresponding to the period in which the major flash flood occurred on 16 October 2022.

Data preprocessing and spatial analysis were performed using Google Earth Engine (GEE), a cloud-based platform for geospatial computation widely adopted for environmental monitoring (Gorelick et al., 2017). Rainfall data were sourced from the Climate Hazards Center InfraRed Precipitation with Station data (CHIRPS), while vegetation indices, land use classification, and topographic data were extracted from Sentinel-2 MSI Level-2A imagery and ALOS PALSAR digital elevation models (DEM). Soil texture, structure, permeability, and organic matter were determined through field sampling and laboratory analysis carried out in 2022. This multi-source data integration enabled robust spatial modeling of soil erosion factors with high accuracy. **Table 1** provides a summary of each dataset and its application in USLE parameter estimation.

Table 1.

Summary of data sources and their uses in soil erosion calculations.

No.	Data	Data Sources	Data Use
1	Daily rainfall during 2022	Climate Hazards Center InfraRed Precipitation with Station data (CHIRPS) analyse by Google Earth Engine (GEE), https://developers.google.com/earth-engine/datasets/catalog/UCSB-CHG_CHIRPS_DAILY	To analyse the rainfall erosivity (*R*) factor
2	Soil properties i.e., (structure, texture, permeability and organic matter)	Field observation and soil laboratory analyst in 2022	To analyse the soil erodibility (*K*) factor
3	Perpendicular Vegetation Index (PVI) and Normalized Difference Senescent Vegetation Index (NDSVI)	Sentinel-2 MSI Level-2A analyse by GEE https://developers.google.com/earth-engine/datasets/catalog/COPERNICUS_S2_SR_HARMONIZED , acquired in 2022	To analyse the vegetation cover (*C*) factor
4	Land use map		To analyse the support practices (*P*) factor
5	Topography	ALOS PALSAR – Radiometric Terrain Correction DEM (12.5 m) free access https://asf.alaska.edu/	To analyse Slope length and steepness factor (*LS*)

3.2. Soil Sampling and Laboratory Analysis

To analyse the soil erodibility (K) factor, soil properties were determined through a combination of field sampling and laboratory analysis. The watershed was stratified into representative land units, and a composite sampling strategy was employed. Within each land unit, five sub-samples were collected from a depth of 0-60 cm. This depth was selected because the areas represent dry land dominated by annual plants, and this layer encompasses the primary rooting zone relevant to soil stability and nutrient cycling. These sub-samples were then thoroughly homogenized to create a single composite sample, ensuring it was representative of the unit.

This process yielded a total of 18 composite samples, each weighing approximately 1 kg. These samples were placed in sealed bags for transport and analysis. Several parameters were measured. Soil structure was determined by visual observation in the field at each sampling site. Soil permeability was measured using undisturbed soil cores collected with a sample ring. In the laboratory, the composite samples were first air-dried. The soil organic matter content was then quantified using the (Walkley & Black, 1934) method. Finally, soil texture was analysed to determine the percentage of sand, silt, and clay, as well as the specific very fine sand (0.1–0.05 mm) and finer silt fractions (0.05–0.02 mm) required by the erodibility equation.

3.3. Soil Erosion Calculations

The Universal Soil Loss Equation (USLE), developed by (W. H. Wischmeier & Smith, 1965) and refined in 1978 (Wischmeier & Smith, 1978), is widely recognized for estimating long-term average annual soil erosion. It enables assessment of erosion risk across landscapes by integrating climatic, topographic, vegetative, and management factors. The general form of the equation is expressed as:

$$\boldsymbol{A = R \times K \times LS \times C \times P} \quad (1)$$

where: A is the estimated soil loss (t ha^{-1} yr^{-1}), R represents the rainfall erosivity factor (MJ mm ha^{-1} h^{-1} yr^{-1}), K is the soil erodibility factor (t ha^{-1} MJ^{-1} mm^{-1}), LS denotes the slope length and steepness factor (dimensionless), C is the cover-management factor (dimensionless), and P is the erosion control practice factor (dimensionless).

a. Rainfall erosivity factor (R)

Rainfall erosivity (R) quantifies the potential of rainfall to detach and transport soil particles. Because continuous, high-resolution precipitation data required for direct EI_{30} calculation are often unavailable in many regions, an empirical model must be used. We calculated the monthly rainfall erosivity using the equation proposed by (Bols, 1978), which is specifically adapted for tropical climates using more readily available meteorological station data (Eq. 2):

$$EI_{30} = 6.119(\mathrm{RAIN})^{1.21} \times (\mathrm{DAYS})^{-0.47} \times (\mathrm{MAXP})^{0.53} \quad (2)$$

EI_{30} represents the monthly rainfall erosivity, $RAIN$ is the average monthly rainfall (cm), $DAYS$ refers to the average number of rainy days in a month, and $MAXP$ denotes the maximum rainfall on a single day within the month (cm). The spatial output was interpolated via kriging to produce a 10 m resolution raster of R values.

b. Soil erodibility factor (K)

The soil erodibility factor (K) measures the inherent susceptibility of a soil to erosion caused by rainfall and surface runoff. It is an integrated measure of how soil properties, such as texture, structure, and composition, collectively resist detachment and transport. The K value was calculated using the following (Eq. 3), which empirically links these key soil properties:

$$100K = 1.292\ [2.1M^{1.14}(10^{-4})(12 - a) + 3.25(b - 2) + 2.5(c - 3)] \quad (3)$$

where: K is the soil erodibility value (t ha^{-1} MJ^{-1} mm^{-1}), M is the percentage of very fine sand (0.1–0.05 mm) and finer fractions (0.05–0.02 mm) multiplied by (100 – the percentage of clay), a is the percentage of organic matter, b is the soil structure code, and c is the soil profile permeability class. Soil data were derived from laboratory tests of samples collected in representative land units.

c. Slope length and steepness factor (LS)

The topographic factor (LS) is calculated as the ratio of soil erosion from a given slope length and steepness to erosion from a standard reference slope. This factor combines two crucial topographic influences: slope length (L), which determines the cumulative volume and velocity of runoff, and slope steepness (S), which primarily controls runoff velocity and the gravitational force acting on soil particles. We calculated the LS factor using the (Eq. 4) proposed by (Moore & Burch, 1986), an approach based on unit stream power theory that is well-suited for distributed modeling with Digital Elevation Models (DEMs).

$$LS = \left(\frac{\text{Flow accumulation} \times \text{Cell size}}{22.13} \right)^{0.4} \times \left(\frac{\sin(\text{Slope})}{0.0896} \right)^{1.3} \quad (4)$$

Topographic inputs (specifically flow accumulation and slope gradient, which are required for Eq. 4) were derived from ALOS PALSAR DEM at 12.5 m resolution, resampled to match the final 10 m analysis grid.

d. Vegetation cover and crop management factor (C)

The C factor represents the ratio of soil erosion from a specific vegetation cover and land management practice to erosion from a continuous bare soil condition. It quantifies the protective effects of vegetation, which include intercepting rainfall, reducing runoff velocity, and binding soil with roots. Because direct field measurements of C are impractical over large areas, we used a remote sensing-based approach to capture the spatial and temporal dynamics of vegetation cover. The C factor was calculated using the algorithm (Eq. 5) developed by (Feng et al., 2018):

$$C = \big(0.681 - (0.523 \times PVI)\big) - (1.255 \times NDSVI) \quad (5)$$

where: PVI is perpendicular vegetation index (Feng et al., 2018; Richardson & Wiegand, 1977). This index is sensitive to the amount of green (photosynthetically active) vegetation, which provides the primary canopy cover against raindrop impact. NDSVI is normalized difference senescent vegetation index (Qi et al., 2002). This index was included to account for the protective cover provided by non-photosynthetic vegetation, such as dry grass or crop residues, which also contribute to soil protection. The formulas for calculating PVI (Eq. 6) and NDSVI (Eq. 7) using Sentinel-2A bands are:

$$PVI = \frac{NIR - (1.088 \times Red) - 0.056}{\sqrt{1.088^2 + 1}} \quad (6)$$

$$NDSVI = \frac{SWIR\ 1 - Red}{SWIR\ 1 + Red} \quad (7)$$

e. Erosion control practice factor (P)

The P factor accounts for the effectiveness of specific conservation practices (such as terracing or contour farming) in reducing runoff and soil loss compared to cultivation without such practices. It is a critical factor that represents the direct human intervention on the landscape to mitigate erosion.

It modifies the erosion potential by altering runoff pathways, slowing water velocity, and trapping sediment. The P factor ranges between 0 (indicating excellent, highly effective erosion control) and 1 (indicating no conservation practice). To account for the combination of different practices found in tropical agricultural landscapes, the P factor was estimated based on the approach proposed by As-syakur et al. (2022), (Eq. 8)

$$P = P_C \times P_T \times P_{CT} \quad (8)$$

where: P_C is the contour farming factor, P_T and P_{CT} are sub-factors for terracing and strip cropping, respectively. The values for these sub-factors depend on land use and slope class. Detailed values can be found in the study by (Adnyana et al., 2024).

To spatially assign the P factor values, we first developed a classification of land management techniques. This classification was based on integrating the land use/land cover map (also used for the C factor) with the slope steepness map (derived from the DEM). A specific value for each sub-factor (P_C, P_T, and P_{CT}) was then assigned to every pixel in the study area using a lookup table. This table links specific land use types (e.g., 'rice paddy', 'mixed agriculture', 'forest') and slope gradient classes (e.g., '0-3%', '3-8%') to a corresponding conservation practice value. For instance, agricultural areas on steep slopes known to be terraced were assigned a low P_T value, while agricultural areas on gentle slopes were evaluated for contour farming (P_C). Following this classification, any land use class identified as having no conservation practices (such as bare land or unmanaged shrubland) was assigned a P value of 1, representing the absence of erosion control.The specific values for each sub-factor (P_C, P_T, and P_{CT}) based on this land use and slope classification were adopted from the detailed tables established for tropical regions in the study by (Adnyana et al., 2024). Finally, the sub-factor rasters were multiplied together (as per Eq. 8) to generate the final P factor map.

3.4. Soil erosion classification

The final step in the analysis was to translate the quantitative soil erosion rates (measured in t/ha/year) into a qualitative hazard assessment. This was achieved by categorizing the final computed soil loss values, which represent the spatial output of the combined R, K, LS, C, and P factors, into five distinct classes. These classification thresholds are not universal; they were specifically based on benchmarks established in prior research conducted in tropical regions (Adnyana et al., 2024; Almagro et al., 2019), making them relevant to the study area's environmental conditions.

The classification is as follows: very light erosion (<1 t/ha/year), light erosion (1–5 t/ha/year), moderate erosion (>5–10 t/ha/year), heavy erosion (>10–50 t/ha/year), and very heavy erosion (>50 t/ha/year). This reclassification process transforms the continuous numerical data into a discrete hazard map. These categories provide a clear and actionable framework for identifying erosion hotspots and prioritizing conservation efforts. The final computed erosion rates and the resulting classified map were standardized to the Universal Transverse Mercator (UTM) Zone 50S projection and represented in a raster format with a spatial resolution of 10 meters. This high-resolution format was maintained throughout the analysis to allow for detailed spatial analysis, enhancing the precision of the final erosion hazard assessment.

3.5. Approach for Mitigation Strategy Identification

It is important to clarify that this study's primary methodological objective was the high-resolution spatial identification of erosion hotspots. This focus was chosen because these are the principal sources of sediment that cause blockage of the main river channel and subsequently drive flash flood events in the Biluk Poh Watershed. By identifying the source of the sediment (the erosion hotspots), our mitigation recommendations are inherently designed to address the root cause of the

river channel blockage and, consequently, the flash flood risk. The research did not involve the field implementation or testing of new conservation structures.

Therefore, the mitigation strategies presented in the discussion section of this paper were identified through a descriptive approach. Following the classification of erosion hazards (as described in section f), we conducted a targeted literature review. This review focused on identifying established soil and water conservation techniques (both vegetative and mechanical) that are effective in not only reducing on-site soil loss but also in trapping sediment and reducing peak runoff, which are the two key processes linking upstream erosion to downstream flooding. Our recommendations are thus based on this synthesis of previous research, specifically targeting interventions suitable for areas classified with moderate to very heavy erosion levels, which correspond to the hotspots identified as the primary contributors to the watershed's sediment load and flood vulnerability.

4. RESULTS

4.1. Rainfall erosivity factor (R)

The rainfall erosivity factor (R) was calculated using CHIRPS satellite precipitation data, extracted from 16 pixels distributed across the watershed (**Fig. 2**). To generate a continuous 10 m resolution raster, the data were interpolated using the kriging method in ArcGIS. The resulting R values ranged from 1,296 to 1,776 MJ mm ha^{-1} h^{-1} yr^{-1} (**Fig. 3**). Spatially, higher erosivity values were concentrated in the upstream region, while the downstream area exhibited lower values. This gradient reflects differences in total annual precipitation, the number of rainy days, and maximum daily rainfall intensity.

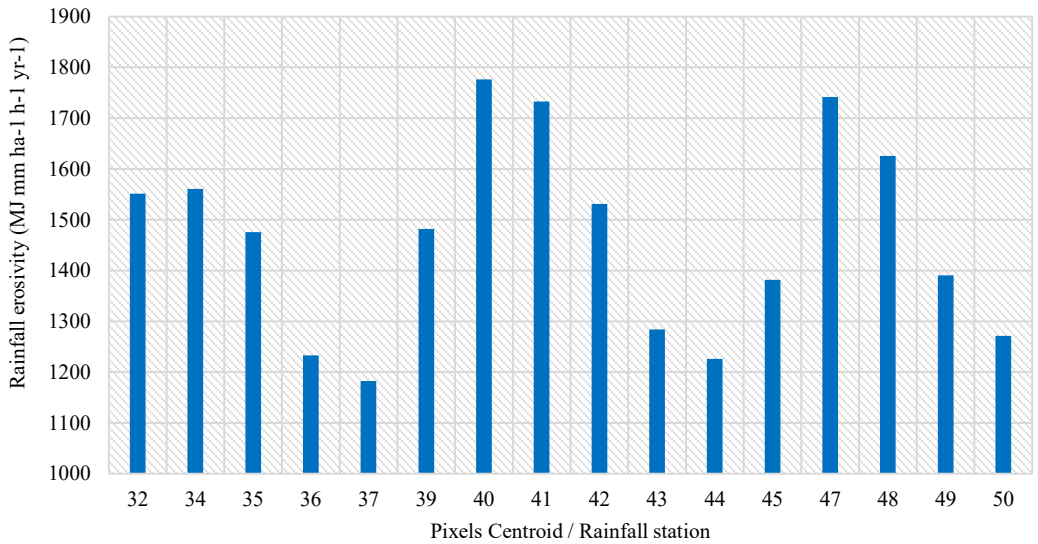

Fig. 2. CHIRPS-derived R factor values from sampled pixels in the study area.

These findings are consistent with (Nikolova et al., 2024), who reported that watersheds with high rainfall erosivity, coupled with poor land management, face elevated erosion risks. Similarly, previous researchers state that linked extreme erosivity patterns in Southeast Asia to climate anomalies such as ENSO, which influence rainfall regimes and storm intensity in tropical regions (Adnyana et al., 2024; Adnyana et al., 2025). The upper portions of the Biluk Poh Watershed thus represent critical erosion-prone zones due to their combined climatic and topographic conditions.

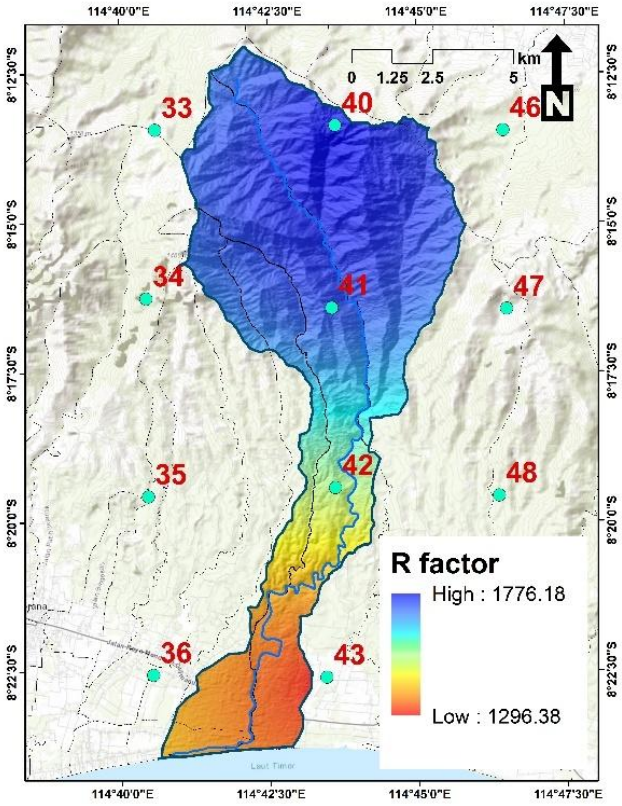

Fig. 3. Interpolated spatial distribution of the R factor across the watershed.

4.2 Soil erodibility factor (K)

The soil erodibility factor (K) quantifies the intrinsic vulnerability of soil to erosion, based on physical and chemical characteristics such as texture, structure, organic matter, and permeability (Renard et al., 2023). K values in the Biluk Poh Watershed ranged from 0.14 to 0.48 t ha h MJ^{-1} mm^{-1}. The most dominant category was moderately high erodibility, covering 70.01% of the area (**Fig. 4**). Spatial analysis indicated that higher K values occurred in the midstream to upstream regions, whereas lower values were found in the flatter, downstream zones (**Fig. 5a**).

These elevated K values were primarily associated with dryland farming and mixed forest systems underlain by Latosol and Litosol soil types. These soils often exhibit poor aggregation, low organic matter, and fine textures that are highly susceptible to detachment. Lal (2001) emphasized that soils with weak structure and poor infiltration capacity are especially prone to erosion under intense rainfall. Previous researchers demonstrated the protective role of vegetation in reducing erodibility by improving soil porosity and root cohesion (J. Liu et al., 2019).

4.3. Slope length and steepness factor (LS)

The LS factor is a dimensionless index that quantifies the combined effect of slope length and slope gradient on erosion potential, relative to a standard reference plot. The resulting LS index values for the Biluk Poh Watershed, which ranged from 0 to 45, were grouped into five classes to map the spatial distribution of topographic vulnerability (**Fig. 5b**).

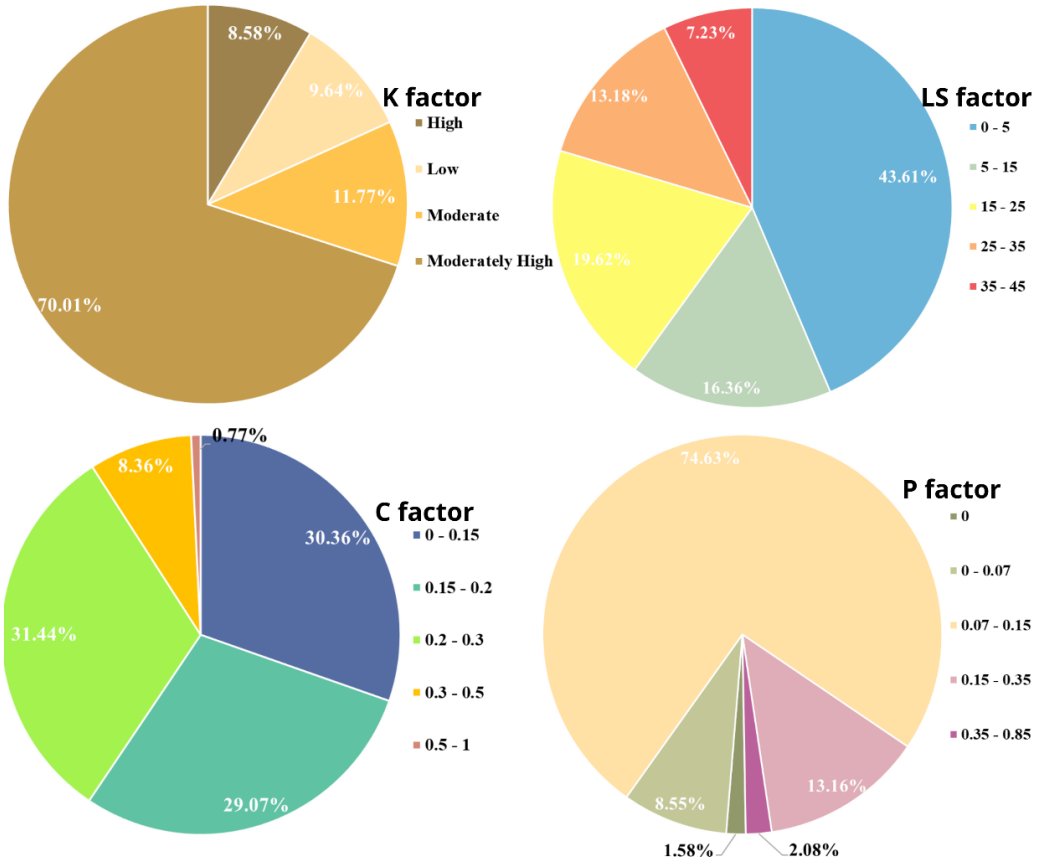

Fig. 4. Percentage Diagram of area coverage for each erosion factor (K, LS, C, and P).

The 0–5 class, representing the lowest topographic vulnerability, dominates 43.61% of the area (**Fig. 4**), corresponding to the flat, downstream alluvial plains. Conversely, the higher-value classes (e.g., 25-35 and 35-45) are concentrated in the upstream regions. In these areas, the high LS values indicate that the combination of steep slopes and long flow paths significantly increases runoff energy and reduces infiltration time, thereby enhancing soil detachment rates. This is in line with findings by (Chaplot & Le Bissonnais, 2003), who showed that slope-induced kinetic energy is a major driver of surface erosion. As stressed by Hou et al. (2021), these upstream regions with the highest LS values are particularly vulnerable and require slope-based conservation interventions such as contour terracing, vegetation reinforcement, and slope stabilization.

4.4. Vegetation Cover and Management Factor (C)

The C factor reflects the effectiveness of vegetation in protecting soil from raindrop impact and surface runoff (Ayalew et al., 2020; Karaburun, 2010). It was calculated using Sentinel-2 imagery, specifically the Perpendicular Vegetation Index (PVI) and Normalized Difference Senescent Vegetation Index (NDSVI), which distinguish between healthy and degraded vegetation. C values ranged from 0 to 1. The watershed was classified into five categories based on C values (**Fig. 5c**). The largest portion of the watershed (31.44%) fell within the 0.2–0.3 class, followed closely by the 0–0.15 class (30.36%) and the 0.15–0.2 class (29.07%). These areas represent moderate to dense vegetation cover with relatively low erosion potential. Conversely, higher C values in the 0.3–0.5 range covered 8.36% of the area, while the highest values (0.5–1) comprised 0.77% (**Fig. 4**).

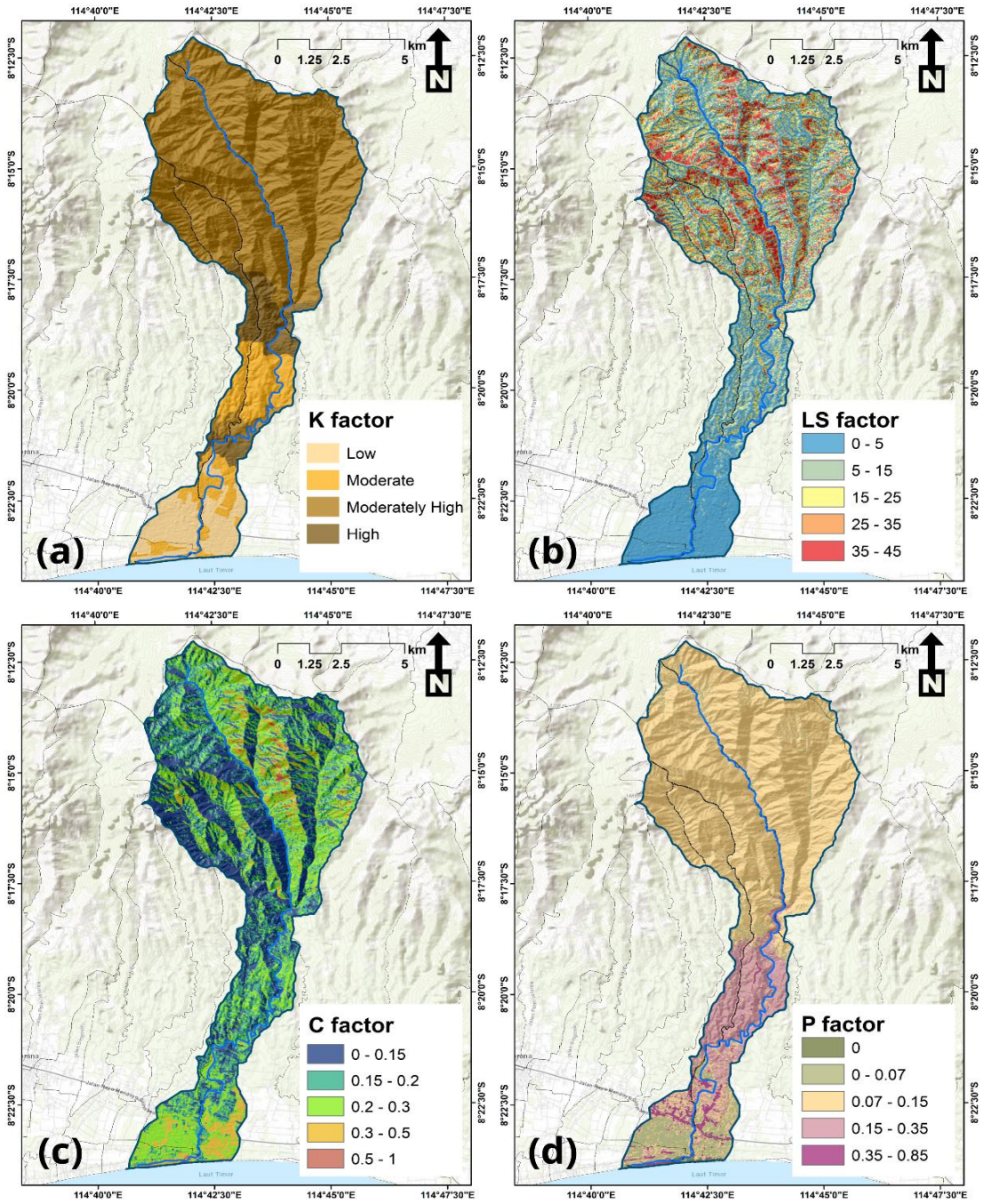

Fig. 5. Spatial distribution of K factor (a), LS factor (b), C factor (c), and P factor (d).

Spatially, a critical finding is the concentration of higher C values (0.3–1) in the upper part of the watershed. These zones, which collectively cover just over 9% of the area, spatially correlate with areas where both dense forest vegetation and annual agriculture are relatively sparse (**Fig. 5c**). This lack of protective cover in the upstream regions is a significant finding, as it leaves soil exposed to raindrop impact and facilitates higher runoff velocities, directly influencing the erosion hotspots

identified in the watershed. These results reinforce previous findings by (Alexakis et al., 2021; Biddoccu et al., 2020), who noted that strong vegetative cover enhances infiltration, binds soil aggregates, and reduces runoff. Targeted reforestation, agroforestry integration, and riparian vegetation rehabilitation in high-C value zones would significantly mitigate erosion vulnerability.

4.5. Conservation practices factor (P)

The conservation practices factor (*P*) represents the extent to which conservation measures reduce soil erosion risk, including techniques such as terracing, conservation tillage, and vegetative cover (Ebabu et al., 2022). Based on the analysis, the P factor values in the Biluk Poh Watershed ranged from 0 to 0.85, with high values spatially dominant in the midstream area of the watershed (**Fig. 5d**). The land area proportions revealed that the most prevalent *P* factor category was 0.07–0.15, covering 74.63% of the total study area, followed by the 0.15–0.35 category, which accounted for 13.16% (**Fig. 4**). High P factor values indicate areas with minimal adoption of conservation practices, particularly on steep slopes. Conversely, areas with low P factor values reflect effective conservation measures, such as the implementation of terracing and vegetative cover. Negese et al. (2021) emphasized the importance of soil conservation practices in reducing erosion, especially on land with steep slopes. Similarly, Panagos et al. (2015) demonstrated that the application of appropriate conservation techniques can reduce erosion risks by up to 70%. The implementing strategies such as terracing and vegetative rehabilitation significantly decreases erosion rates in vulnerable areas (Dharmawan et al., 2023; Nugroho et al., 2022).

4.6. Soil erosion hotspot

Soil erosion remains one of the most critical land degradation processes threatening agricultural productivity, ecological stability, and the long-term sustainability of tropical watersheds. In the Biluk Poh Watershed, high-resolution spatial modeling using remote sensing data, field observations, and laboratory analyses revealed significant variation in annual erosion rates, ranging from 0 to 4664.78 t ha^{-1} yr^{-1}, with an average rate of 168.03 t ha^{-1} yr^{-1}. This heterogeneity reflects the combined influence of rainfall erosivity, topographic steepness, land cover dynamics, and land management practices, as also noted in Mediterranean and tropical landscapes (Panagos et al., 2015). Erosion classification revealed that Slight erosion (0–15 t ha^{-1} yr^{-1}) dominated the watershed, covering 39.30% of the area. This was followed by the Heavy class (180–480 t ha^{-1} yr^{-1}) at 29.42%, the Moderate class (60–180 t ha^{-1} yr^{-1}) at 18.56%, the Very Heavy class (>480 t ha^{-1} yr^{-1}) at 7.99%, and the Light class (15–60 t ha^{-1} yr^{-1}) covering 0.73% (**Fig. 6**), underscoring the spatial complexity of erosion processes.

While the Very Heavy erosion category constitutes a relatively small portion of the total area at 7.99%, it represents a critical baseline finding due to its spatial distribution. The highest erosion intensities were concentrated in the midstream to upstream regions, particularly along steep slopes and fluvial corridors that exhibited both high LS values and low vegetation cover. These zones, depicted in orange to red on the erosion map (**Fig. 7**), are characterized by accelerated overland flow and sediment detachment during periods of intense rainfall. The strategic location of these hotspots means that eroded material can be delivered directly into the main river, posing a significant risk of blockage. The October 2022 flash flood event exemplified how this upstream erosion hotspots can rapidly deliver sediment into the main river channel, resulting in reduced discharge capacity and triggering downstream inundation. At the village scale, the erosion hazard was most acute in Penyaringan and Yeh Embang Kauh, with 11.95% and 13.39% of their land areas, respectively, falling within the heavy erosion class (**Fig. 6**). These areas share common characteristics, including steep terrain, weakly aggregated soils, and minimal conservation infrastructure, making them high-priority zones for erosion mitigation. The erosion hazard maps highlight these critical microzones, emphasizing the need for site-specific interventions such as slope stabilization, vegetative ground cover, and improved runoff diversion and drainage systems.

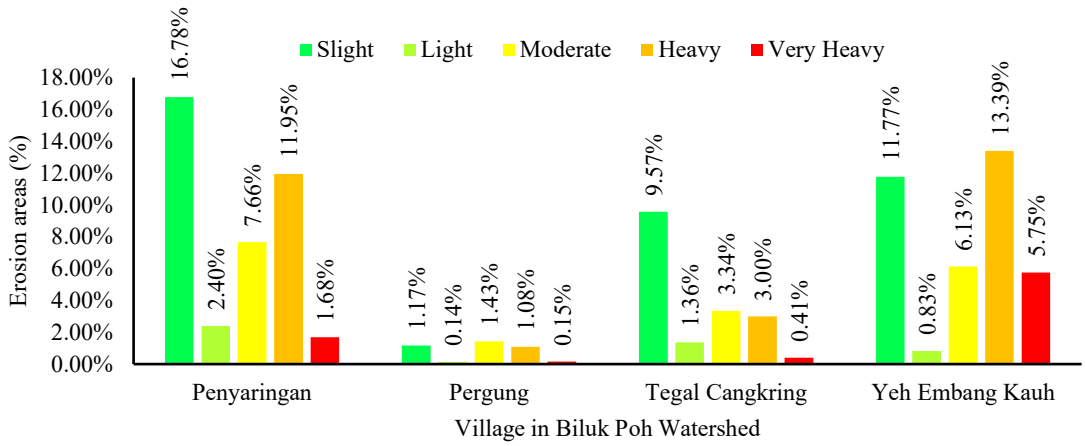

Fig. 6. Village areas surrounding the watershed based on the extent of erosion hazard levels.

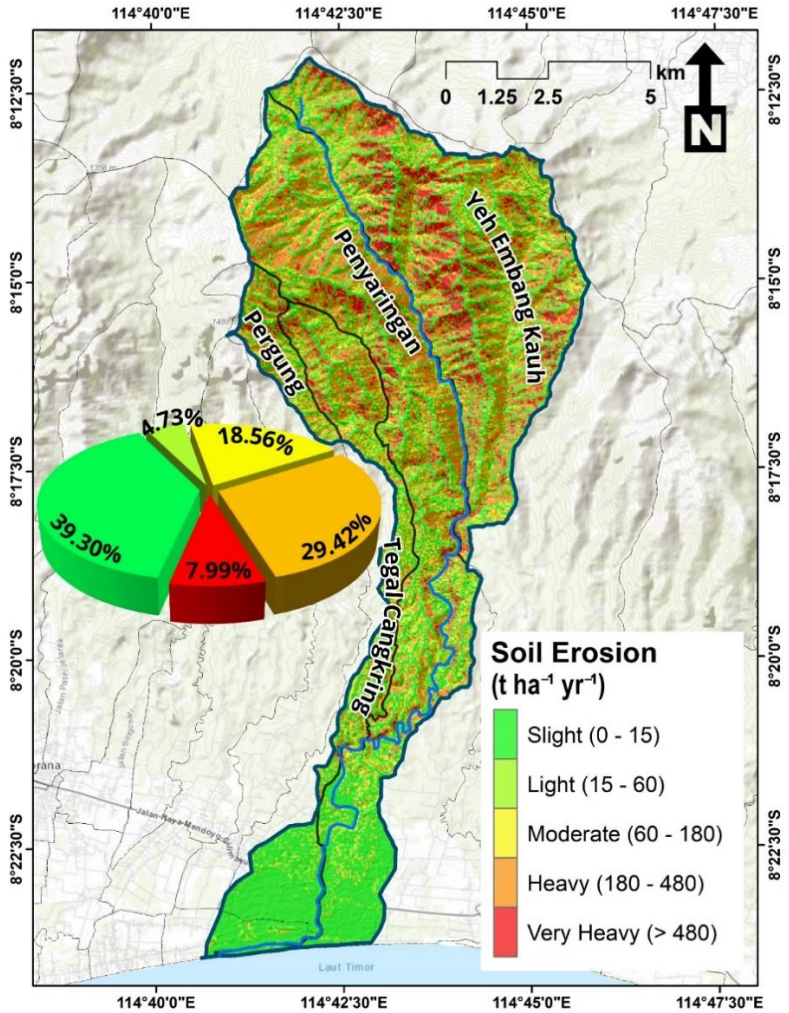

Fig. 7. Spatial distribution of soil erosion hazard along with area percentages.

5. DISCUSSION

Evidence from surrounding regions in Bali corroborates the patterns observed in Biluk Poh. Trigunasih & Saifulloh (2023) documented erosion rates ranging from 20.17 to 995.48 t ha^{-1} yr^{-1} in nearby watersheds, while (Trigunasih et al., 2018; Trigunasih & Saifulloh, 2022) reported rates between 0.32 and 1,535.34 t ha^{-1} yr^{-1} in the Penet Watershed. These findings underscore the influence of terrain morphology and anthropogenic land use on spatial erosion risk. Additionally, (Diara et al., 2022, 2023; Suyarto et al., 2023) emphasized that the Baturiti Highlands and adjacent uplands face dual threats from erosion and shallow landslides due to deforestation on steep volcanic slopes.

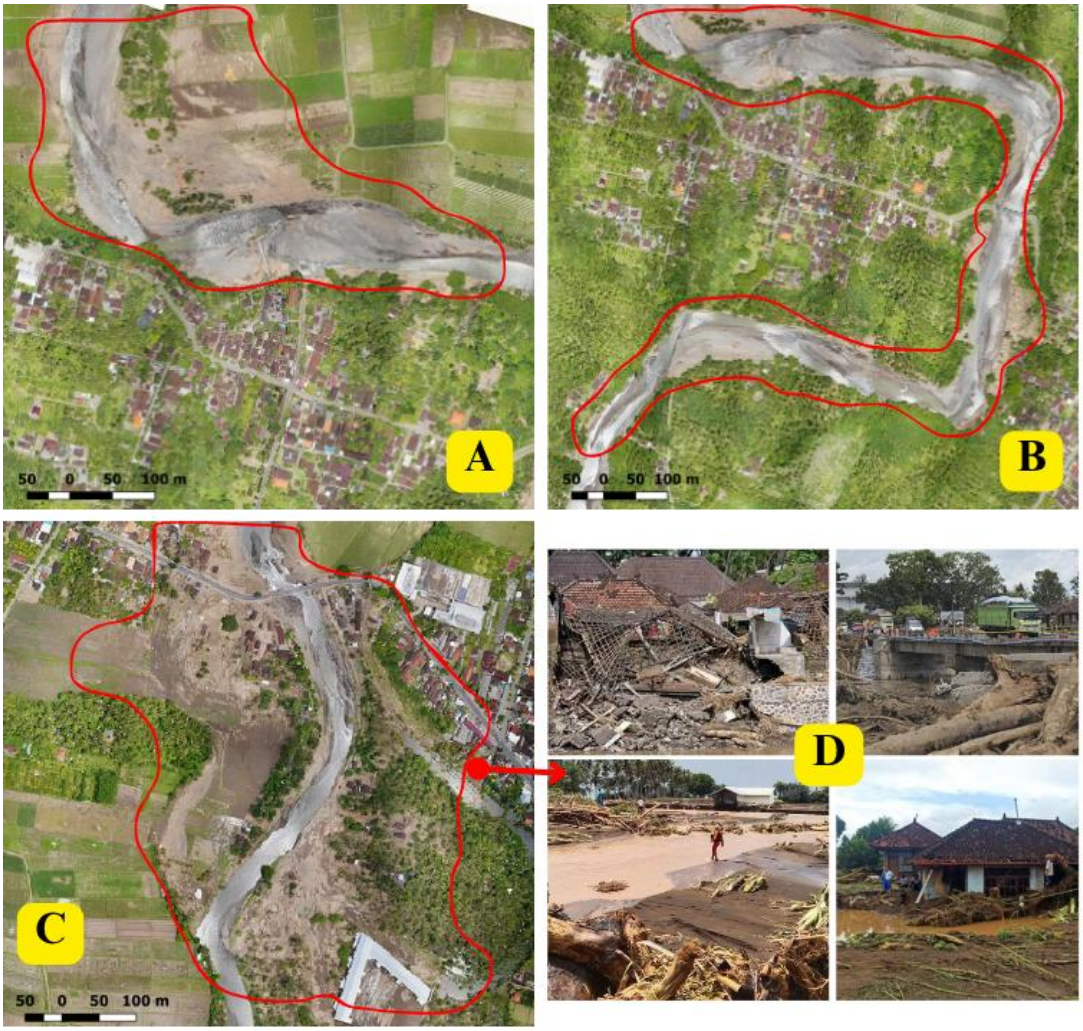

Fig. 8. Aerial and ground views of erosion-affected areas and flash flood damage in the Biluk Poh Watershed. (A-C) Sediment accumulation and slope failure in downstream and midstream zones. (D) Infrastructure damage and debris after the 16 October 2022 flood.

From a soil perspective, Bali's dominant Entisols are particularly vulnerable to erosion due to their sandy texture and low aggregate stability (Araújo Filho et al., 2021; G. Liu et al., 2009). This vulnerability is supported by findings in the Telagawaja Sub-Watershed, where (Soniari et al., 2024) reported moderate to high erodibility (K) values. The consequences of this susceptibility extend

beyond physical degradation; studies have confirmed that erosion results in significant nutrient depletion especially nitrogen, phosphorus, and soil organic carbon thereby undermining long-term soil fertility (Kartini et al., 2023, 2024; Trigunasih et al., 2023).

This study contributes to the field by applying a 10-meter resolution raster-based erosion model, enabling fine-scale detection of erosion-prone microzones. In contrast to conventional methods that rely on homogeneous land units, this pixel-based approach captures detailed spatial variability, which is essential for managing complex landscapes like Biluk Poh, where topographic and land-use changes occur over short distances.

The watershed's geomorphological characteristics further intensify its susceptibility to hydrological extremes (Soniari et al., 2024). Its radial drainage pattern, consisting of multiple upstream tributaries converging into a single outlet, creates a discharge bottleneck during high rainfall events. In October 2022, rainfall increased by 79.78% from the previous month, with several days exceeding critical thresholds. This surge led to rapid runoff and widespread soil detachment in slope-dominant regions. The C factor analysis confirmed substantial degradation of vegetative cover in these zones, weakening the land's capacity to intercept rainfall and retain soil particles (J. Liu et al., 2019). UAV imagery from post-flood assessments (**Fig. 8A-C)** revealed bare hillslopes, riverbank collapse, and sediment deposition in key river sections (**Fig. 8D**), corroborating the spatial accuracy of the modeled erosion data. These observations affirm that soil erosion not only degrades land productivity but also acts as a precursor to flash flood disasters. Sediments mobilized from unstable upstream areas accumulated in constricted river segments, obstructing flow and intensifying flooding impacts. Field documentation revealed widespread damage to farmland, transportation infrastructure, and riverbanks, validating the sedimentation pathways identified in the erosion model.

A closer analysis of the spatial erosion map (**Fig. 7**) provides the quantitative basis for this sediment mobilization. The model revealed extreme erosion values reaching up to 4664.78 t ha^{-1} yr^{-1} in localized hotspots. More critically, the combined area of the Heavy (29.42%) and Very Heavy (7.99%) erosion classes covers 37.41% of the watershed. These high-risk zones are not randomly distributed; they form a contiguous network concentrated along the steep fluvial corridors and denuded slopes identified in the upstream and midstream regions. This specific geographic arrangement creates a highly efficient delivery system, funneling detached soil directly into the main river. This process of rapid, large-scale sediment loading is the primary driver of the channel blockages and reduced discharge capacity that were directly responsible for the 2022 flash flood event.

The broader relevance of these findings is underscored by the recent large-scale flooding in Bali during September 2025. This catastrophic event, which caused widespread damage to key tourism, industrial, and capital areas, was extensively documented by international media and humanitarian organizations (e.g., BBC Weather, 2025; ClimaMeter, 2025; DW News, 2025; IFRC, 2025; The Guardian, 2025). Preliminary reports indicate a familiar pattern: intense, sustained rainfall acting upon watersheds compromised by degraded upstream vegetation, leading to critical blockages in main river channels. While the 2025 disaster was compounded by urban drainage inadequacies, it demonstrates that the core mechanism of sediment-driven channel blockage, as modeled in Biluk Poh, is not an isolated issue but a primary, recurrent, and escalating threat to the entire region. This context lends a new and critical urgency to implementing the mitigation strategies proposed in this paper.

Conservation strategies in the Biluk Poh watershed must therefore address both physical land degradation and the associated loss of soil fertility to support a sustainable agroecosystem (Bhayunagiri & Saifulloh, 2022; Kartini et al., 2023, 2024; Susila et al., 2024). This is critical, as soil erosion leads to the significant depletion of key agricultural nutrients, including nitrogen, phosphorus, and soil organic carbon (Trigunasih et al., 2023). This nutrient depletion directly threatens crop yields, necessitating interventions that protect both the environment and agricultural livelihoods. In this context, the study's application of multi-temporal Sentinel-2 imagery proved highly effective. By enabling a detailed calculation of the C factor, the Sentinel-2 data was instrumental in identifying the specific erosion hotspots where poor or degraded vegetation cover corresponds with high soil loss risk. This methodological approach, which connects the dynamic state of vegetation directly to soil

protection, provides the precise spatial information needed for implementing targeted, climate-smart land management (Plybour et al., 2025; Laosuwan et al., 2025) in the vulnerable microzones of Biluk Poh.

Mitigation of these hazards requires a holistic watershed management approach. Based on the erosion hazard map developed in this study, a clear prioritization of these efforts is possible. Interventions must be focused on the most impacted zones. These were identified as the moderate erosion class (covering 18.56% of the area), the heavy erosion class (affecting 29.42%), and the very heavy erosion class (covering 7.99%). Cumulatively, the moderate and heavy classes represent the most widespread threat, covering a combined 47.98% of the watershed. These areas, combined with the substantial and highly intense very heavy hotspots (7.99%), function as the primary sediment sources for the entire watershed. Treating them is the most direct way to prevent the river channel blockage that causes flash floods.

For the most severe hotspots, particularly the very heavy class and the steepest slopes within the heavy erosion class, reforestation using native deep-rooted species such as *Samanea saman* and *Cassia siamea* is recommended. This provides slope stability at the source, preventing the initial soil detachment (Escalante & Messa, 2023; Maridi et al., 2015). Simultaneously, riparian zones bordering all critical sediment-source areas should be reinforced with *Bambusa* spp. and *Chrysopogon zizanioides* (vetiver grass). This acts as a 'last line of defense' to trap sediment that does mobilize and keep it from reaching the main river channel, thereby reducing bank erosion and sediment accumulation downstream.

For the widespread moderate and heavy erosion areas, which often overlap with agricultural land, a combination of agroforestry and structural measures is essential. Agroforestry systems (60-70% native trees, 30-40% crops) are recommended for 25-45% slopes to balance ecological function and economic productivity (Budiastuti et al., 2020; Kaur et al., 2023). Additionally, contour terracing and vegetative ground cover are crucial. These practices work by slowing runoff velocity, which dramatically reduces the water's power to carry sediment, and by enhancing infiltration, which reduces the total volume of surface runoff that causes the river to swell (Fajeriana et al., 2024).

The integration of high-resolution remote sensing, erosion modeling, and field validation has revealed the spatial extent and severity of erosion across the Biluk Poh Watershed. These findings offer a critical evidence base for implementing these spatially targeted, ecologically sound conservation strategies. By prioritizing interventions in the identified moderate, heavy, and very heavy erosion hotspots, stakeholders can systematically reduce sediment loads at their source and, in turn, enhance watershed resilience and mitigate the long-term risks associated with sediment-driven flash flood events.

6. CONCLUSIONS

The catastrophic flash flood of October 16, 2022, was triggered by intense rainfall, but its severity was critically exacerbated by widespread soil erosion within the Biluk Poh Watershed. This study provides the first rapid geospatial identification of the erosion hotspots that functioned as the principal spatial factors amplifying the disaster.

Our high-resolution analysis revealed that 55.97% of the watershed is susceptible to moderate (18.56%), heavy (29.42%), or very heavy (7.99%) erosion. These hotspots are concentrated in steep upstream and riparian landscapes characterized by high slope gradients, highly erodible soils, inadequate vegetative cover, and limited conservation practices. During the rainfall event, these vulnerable areas mobilized massive sediment loads, leading to the channel aggradation and blockage that worsened downstream flooding. The strong spatial correlation between our modeled hotspots and the flood-damaged areas, confirmed by post-flood UAV imagery, demonstrates that this uncontrolled erosion was a major contributor to the disaster's scale.

The findings from this study provide actionable insights for targeted mitigation. The identification of these erosion-prone microzones confirms the need for an integrated watershed-scale conservation strategy, prioritizing reforestation, agroforestry, and riparian buffers in the identified

risk zones. This research highlights the critical importance of incorporating soil erosion as an exacerbating factor in tropical flood risk management to build resilience against future sediment-driven disasters.

ACKNOWLEDGEMENTS

We sincerely thank the Fly for Humanity Movement for their generous support. Special appreciation is extended to Septian Firmansyah (Sky Volunteer/Synersia) for his key role in aerial data acquisition and to Dewa Putu A. M. from the SIAP SIAGA program (Australia–Indonesia Partnership for Disaster Risk Management) for his valuable assistance. We also gratefully acknowledge the Aviation Technology Research Center of the National Research and Innovation Agency (BRIN) for providing technical expertise and high-resolution aerial imagery, and the Bali Provincial Disaster Management Agency (BPBD Bali) for facilitating field operations and logistics.

FUNDING

This research was financially supported by Universitas Udayana through the DIPA PNBP Fiscal Year 2024 (Research Assignment Agreement No. B/255.614/UN14.4.A/PT.01.03/2024, dated 17 April 2024) and the DIPA PNBP Fiscal Year 2025 (Research Assignment Agreement No. B/229.51/UN14.4.A/PT.01.03/2025, dated 28 April 2025).

REFERENCES

Abu El-Magd, S. A., Orabi, H. O., Ali, S. A., Parvin, F., & Pham, Q. B. (2021). An integrated approach for evaluating the flash flood risk and potential erosion using the hydrologic indices and morpho-tectonic parameters. *Environmental Earth Sciences*, *80*(20). https://doi.org/10.1007/s12665-021-10013-0

Addy, S., & Wilkinson, M. E. (2021). Embankment lowering and natural self-recovery improves river-floodplain hydro-geomorphic connectivity of a gravel bed river. *Science of the Total Environment*, *770*. https://doi.org/10.1016/j.scitotenv.2020.144626

Adnyana, I. W. S., As-syakur, A. R., Suyarto, R., Sunarta, I. N., Nuarsa, I. W., Diara, I. W., Saifulloh, M., & Wiyanti. (2024). Geospatial Technology for Climate Change: Influence of ENSO and IOD on Soil Erosion. In *Technological Approaches for Climate Smart Agriculture* (pp. 249–275). Springer.

Ahrendt, S., Horner-Devine, A. R., Collins, B. D., Morgan, J. A., & Istanbulluoglu, E. (2022). Channel Conveyance Variability can Influence Flood Risk as Much as Streamflow Variability in Western Washington State. *Water Resources Research*, *58*(6). https://doi.org/10.1029/2021WR031890

Alexakis, D. D., Manoudakis, S., Agapiou, A., & Polykretis, C. (2021). Towards the assessment of soil-erosion-related c-factor on european scale using google earth engine and sentinel-2 images. *Remote Sensing*, *13*(24). https://doi.org/10.3390/rs13245019

Almagro, A., Thomé, T. C., Colman, C. B., Pereira, R. B., Marcato Junior, J., Rodrigues, D. B. B., & Oliveira, P. T. S. (2019). Improving cover and management factor (C-factor) estimation using remote sensing approaches for tropical regions. *International Soil and Water Conservation Research*, *7*(4). https://doi.org/10.1016/j.iswcr.2019.08.005

Ao, L., Wu, Y., Xu, Q., Zhou, Y., Chen, X., Liang, P., Fu, Z., & Chen, H. (2025). The Role of Bedrock Topography in the Runoff Process and Soil Erosion on Karst Steep Slopes. *Land Degradation & Development*, *36*(2), 533–544.

Araújo Filho, R. N., Holanda, F. S. R., Cunha Filho, M., Piscoya, V. C., MELO, J. D. E. O., & Guimarães, D. V. (2021). Relationship between physical and chemical properties of entisols-fluvents and erosion in the sao francisco river. *Revista Caatinga*, *34*(2), 422–431.

As-syakur, A. R., Adnyana, I. W. S., & Osawa, T. (2022). (2022). *Erosion prediction based on USLE*

method using remote sensing data and GIS in small scale watershed.

Ayalew, D. A., Deumlich, D., Šarapatka, B., & Doktor, D. (2020). Quantifying the sensitivity of NDVI-based C Factor Estimation and Potential Soil Erosion Prediction using Spaceborne Earth Observation Data. *Remote Sensing*, *12*(7). https://doi.org/10.3390/rs12071136

BBC Weather. (2025). Bali flash floods report. BBC News. https://www.bbc.com/weather/articles/cevzegvjw7jo

Bauer, M., Dostal, T., Krasa, J., Jachymova, B., David, V., Devaty, J., Strouhal, L., & Rosendorf, P. (2019). Risk to residents, infrastructure, and water bodies from flash floods and sediment transport. *Environmental Monitoring and Assessment*, *191*(2). https://doi.org/10.1007/s10661-019-7216-7

Bhayunagiri, I. B. P., & Saifulloh, M. (2022). Mapping of subak area boundaries and soil fertility for agricultural land conservation. *Geographia Technica*, *17*(2). https://doi.org/10.21163/GT_2022.172.17

Biddoccu, M., Guzmán, G., Capello, G., Thielke, T., Strauss, P., Winter, S., Zaller, J. G., Nicolai, A., Cluzeau, D., Popescu, D., Bunea, C., Hoble, A., Cavallo, E., & Gómez, J. A. (2020). Evaluation of soil erosion risk and identification of soil cover and management factor (C) for RUSLE in European vineyards with different soil management. *International Soil and Water Conservation Research*, *8*(4). https://doi.org/10.1016/j.iswcr.2020.07.003

Bols, P. L. (1978). The iso-erodent map of Java and Madura. *Soil Res. Inst. Bogor*.

Budiastuti, M. T. S., Purnomo, D., Hendro, H., Sudjianto, U., & Gunawan, B. (2020). Rehabilitation of critical land by Implementing complex agroforestry at the prioritized subwatersheds in the Muria Region. *Sains Tanah*, *17*(1). https://doi.org/10.20961/stjssa.v17i1.37704

Chaplot, V. A. M., & Le Bissonnais, Y. (2003). Runoff Features for Interrill Erosion at Different Rainfall Intensities, Slope Lengths, and Gradients in an Agricultural Loessial Hillslope. *Soil Science Society of America Journal*, *67*(3). https://doi.org/10.2136/sssaj2003.8440

Chen, X., Tian, S., Chen, N., Hu, G., Hou, R., & Peng, T. (2024). Why did localized extreme rainfall trigger a rare mega flash flood in the mountains of western China? *International Journal of Disaster Risk Reduction*, 105090.

ClimaMeter. (2025). Bali floods September 9-10, 2025. ClimaMeter. https://www.climameter.org/20250909-10-bali-floods

Dharmawan, I. W. S., Pratiwi, Siregar, C. A., Narendra, B. H., Undaharta, N. K. E., Sitepu, B. S., Sukmana, A., Wiratmoko, M. D. E., Abywijaya, I. K., & Sari, N. (2023). Implementation of Soil and Water Conservation in Indonesia and Its Impacts on Biodiversity, Hydrology, Soil Erosion and Microclimate. In *Applied Sciences (Switzerland)* (Vol. 13, Issue 13). https://doi.org/10.3390/app13137648

Diara, I. W., Suyarto, R., & Saifulloh, M. (2022). Spatial distribution of landslide susceptibility in new road construction Mengwitani-Singaraja, Bali-Indonesia: based on geospatial data. *International Journal of GEOMATE*, *23*(96). https://doi.org/10.21660/2022.96.3320

Diara, I. W., Wahyu Wiradharma, I. K. A., Suyarto, R., Wiyanti, W., & Saifulloh, M. (2023). Spatio-temporal of landslide potential in upstream areas, Bali tourism destinations: remote sensing and geographic information approach. *Journal of Degraded and Mining Lands Management*, *10*(4). https://doi.org/10.15243/jdmlm.2023.104.4769

Dou, X., Ma, X., Zhao, C., Li, J., Yan, Y., & Zhu, J. (2022). Risk assessment of soil erosion in Central Asia under global warming. *Catena*, *212*, 106056.

DW News. (2025). Indonesia: 19 dead after flash floods. Deutsche Welle. https://www.dw.com/en/indonesia-19-dead-after-flash-floods/a-73959609

Dzwairo, R., Singh, S. K., & Patel, A. (2025). Soil erosion susceptibility assessment through morphometric analysis and morphotectonic implications in Rietspruit sub-basin, South Africa. *Environment, Development and Sustainability*, *27*(7), 16503–16524.

Ebabu, K., Tsunekawa, A., Haregeweyn, N., Tsubo, M., Adgo, E., Fenta, A. A., Meshesha, D. T., Berihun, M. L., Sultan, D., Vanmaercke, M., Panagos, P., Borrelli, P., Langendoen, E. J., & Poesen, J. (2022). Global analysis of cover management and support practice factors that control soil erosion and conservation. In *International Soil and Water Conservation Research* (Vol. 10, Issue 2). https://doi.org/10.1016/j.iswcr.2021.12.002

Escalante, E. E., & Messa, H. F. (2023). Silvopastoral Systems with Native Tree Species in Venezuela. In *Silvopastoral systems of Meso America and Northern South America*. https://doi.org/10.1007/978-3-031-43063-3_12

Fajeriana, N., Ali, A., & Rini, R. P. (2024). Soil Tillage and Planting Along the Contour on Sloping Land to Minimize the Potential for Erosion and Surface Runoff. *Sarhad Journal of Agriculture*, *40*(1). https://doi.org/10.17582/journal.sja/2024/40.1.82.93

Feng, Q., Zhao, W., Ding, J., Fang, X., & Zhang, X. (2018). Estimation of the cover and management factor based on stratified coverage and remote sensing indices: a case study in the Loess Plateau of China. *Journal of Soils and Sediments*, *18*(3). https://doi.org/10.1007/s11368-017-1783-4

Gorelick, N., Hancher, M., Dixon, M., Ilyushchenko, S., Thau, D., & Moore, R. (2017). Google Earth Engine: Planetary-scale geospatial analysis for everyone. *Remote Sensing of Environment*, *202*. https://doi.org/10.1016/j.rse.2017.06.031

Gwapedza, D., Hughes, D. A., Slaughter, A. R., & Mantel, S. K. (2021). Temporal influences of vegetation cover (C) dynamism on MUSLE sediment yield estimates: NDVI evaluation. *Water*, *13*(19), 2707.

Hirabayashi, Y., Alifu, H., Yamazaki, D., Imada, Y., Shiogama, H., & Kimura, Y. (2021). Anthropogenic climate change has changed frequency of past flood during 2010-2013. *Progress in Earth and Planetary Science*, *8*(1). https://doi.org/10.1186/s40645-021-00431-w

Hou, T., Filley, T. R., Tong, Y., Abban, B., Singh, S., Papanicolaou, A. N. T., Wacha, K. M., Wilson, C. G., & Chaubey, I. (2021). Tillage-induced surface soil roughness controls the chemistry and physics of eroded particles at early erosion stage. *Soil and Tillage Research*, *207*. https://doi.org/10.1016/j.still.2020.104807

International Federation of Red Cross and Red Crescent Societies (IFRC). (2025). Field Report: Indonesia: Floods (17886). https://go.ifrc.org/field-reports/17886

Karaburun, A. (2010). Estimation of C factor for soil erosion modeling using NDVI in Buyukcekmece watershed. *Ozean Journal of Applied Sciences*, *3*(1).

Kardhana, H., Wijayasari, W., & Rohmat, F. I. W. (2024). Assessing basin-wide soil erosion in the Citarum watershed using USLE method. *Results in Engineering*, *22*, 102130.

Kartini, N. L., Saifulloh, M., Trigunasih, N. M., & Narka, I. W. (2023). Assessment of Soil Degradation Based on Soil Properties and Spatial Analysis in Dryland Farming. *Journal of Ecological Engineering*, *24*(4). https://doi.org/10.12911/22998993/161080

Kartini, N. L., Saifulloh, M., Trigunasih, N. M., Sukmawati, N. M. S., & Mega, I. (2024). Impact of Long-Term Continuous Cropping on Soil Nutrient Depletion. *Ecological Engineering & Environmental Technology (EEET)*, *25*(11).

Kaur, A., Paruchuri, R. G., Nayak, P., Devi, K. B., Upadhyay, L., Kumar, A., Pancholi, R., & Yousuf, M. (2023). The Role of Agroforestry in Soil Conservation and Sustainable Crop Production: A Comprehensive Review. *International Journal of Environment and Climate Change*, *13*(11). https://doi.org/10.9734/ijecc/2023/v13i113478

Lai, R., Li, J., Wang, P., Guo, Y., Xu, L., Zhang, X., Wang, M., & Zhang, X. (2024). Cumulative sedimentation hazard map of urban areas subject to hyperconcentrated flash flood: A case study of Suide County in the Wuding River basin, China. *Journal of Flood Risk Management*, e12996.

Lal, R. (2001). Soil degradation by erosion. *Land Degradation and Development*, *12*(6). https://doi.org/10.1002/ldr.472

Lamane, H., Mouhir, L., Zouahri, A., Baghdad, B., El Bilali, A., & Moussadek, R. (2025). Modeling soil erosion and sediment yield under climate change: a comparison of RUSLE and MUSLE integrated with SDR using variable soil data resolutions. *Modeling Earth Systems and Environment*, *11*(5), 1–29.

Liu, G., Li, L., Wu, L., Wang, G., Zhou, Z., & Du, S. (2009). Determination of soil loss tolerance of an entisol in Southwest China. *Soil Science Society of America Journal*, *73*(2), 412–417.

Liu, J., Zhang, X., & Zhou, Z. (2019). Quantifying effects of root systems of planted and natural vegetation on rill detachment and erodibility of a loessial soil. *Soil and Tillage Research*, *195*. https://doi.org/10.1016/j.still.2019.104420

Mahmood, S., Naeem, N., Ahamad, M. I., Tariq, Z., & Song, J. (2024). Spatial modeling of soil erosion potential

in the Panjkora Basin, Eastern Hindu Kush: integrated RUSLE and geospatial approaches. *Environment, Development and Sustainability*, 1–22.

Maridi, Agustina, P., & Saputra, A. (2015). Potential Vegetation for Soil and Water Conservation : Case Study in Samin Watershed , Central Java. *International Conference on Science, Technology and Humanit*, *December*.

Merten, J., Stiegler, C., Hennings, N., Purnama, E. S., Röll, A., Agusta, H., Dippold, M. A., Fehrmann, L., Gunawan, D., Hölscher, D., Knohl, A., Kückes, J., Otten, F., Zemp, D. C., & Faust, H. (2020). Flooding and land use change in Jambi Province, Sumatra: Integrating local knowledge and scientific inquiry. *Ecology and Society*, *25*(3). https://doi.org/10.5751/ES-11678-250314

Milazzo, F., Francksen, R. M., Zavattaro, L., Abdalla, M., Hejduk, S., Enri, S. R., Pittarello, M., Price, P. N., Schils, R. L. M., & Smith, P. (2023). The role of grassland for erosion and flood mitigation in Europe: A meta-analysis. *Agriculture, Ecosystems & Environment*, *348*, 108443.

Moore, I. D., & Burch, G. J. (1986). Physical Basis of the Length-slope Factor in the Universal Soil Loss Equation. *Soil Science Society of America Journal*, *50*(5). https://doi.org/10.2136/sssaj1986.03615995005000050042x

Negese, A., Fekadu, E., & Getnet, H. (2021). Potential Soil Loss Estimation and Erosion-Prone Area Prioritization Using RUSLE, GIS, and Remote Sensing in Chereti Watershed, Northeastern Ethiopia. *Air, Soil and Water Research*, *14*. https://doi.org/10.1177/1178622120985814

Nikolova, V., Nikolova, N., Stefanova, M., & Matev, S. (2024). Annual and Seasonal Characteristics of Rainfall Erosivity in the Eastern Rhodopes (Bulgaria). *Atmosphere*, *15*(3). https://doi.org/10.3390/atmos15030338

Nugroho, H. Y. S. H., Basuki, T. M., Pramono, I. B., Savitri, E., Purwanto, Indrawati, D. R., Wahyuningrum, N., Adi, R. N., Indrajaya, Y., Supangat, A. B., Putra, P. B., Auliyani, D., Priyanto, E., Yuwati, T. W., Pratiwi, Narendra, B. H., Sukmana, A., Handayani, W., Setiawan, O., & Nandini, R. (2022). Forty Years of Soil and Water Conservation Policy, Implementation, Research and Development in Indonesia: A Review. In *Sustainability (Switzerland)* (Vol. 14, Issue 5). https://doi.org/10.3390/su14052972

Okacha, A., & Salhi, A. (2024). Refining erosion assessment with NDVI-based modeling: a case study in diverse climatic zones. *Mediterranean Geoscience Reviews*, *6*(3), 219–232.

Othman, A., El-Saoud, W. A., Habeebullah, T., Shaaban, F., & Abotalib, A. Z. (2023). Risk assessment of flash flood and soil erosion impacts on electrical infrastructures in overcrowded mountainous urban areas under climate change. *Reliability Engineering and System Safety*, *236*. https://doi.org/10.1016/j.ress.2023.109302

Panagos, P., Borrelli, P., Meusburger, K., Alewell, C., Lugato, E., & Montanarella, L. (2015). Estimating the soil erosion cover-management factor at the European scale. *Land Use Policy*, *48*. https://doi.org/10.1016/j.landusepol.2015.05.021

Panagos, P., Matthews, F., Patault, E., De Michele, C., Quaranta, E., Bezak, N., Kaffas, K., Patro, E. R., Auel, C., & Schleiss, A. J. (2024). Understanding the cost of soil erosion: An assessment of the sediment removal costs from the reservoirs of the European Union. *Journal of Cleaner Production*, *434*, 140183.

Plybour, C., Uttaruk, Y., Jeefoo, P., Laosuwan, N., & Laosuwan, T. (2025). Spatial drought occurrence and distribution using data from Sentinel-2 satellite and vegetation indices. *Geographia Technica*, *20*(1).

Prasad, B., Tiwari, H. L., Garia, S., Dwivedi, V., & Mishra, K. (2024). A comparative study on the modeling of soil erosion by USLE, RUSLE, and USPED. *ISH Journal of Hydraulic Engineering*, *30*(4), 501–510.

Qi, J., Marsett, R., Heilman, P., Biedenbender, S., Moran, S., Goodrich, D., & Weltz, M. (2002). RANGES improves satellite-based information and land cover assessments in Southwest United States. *Eos*, *83*(51). https://doi.org/10.1029/2002EO000411

Rashmi, I., Karthika, K. S., Roy, T., Shinoji, K. C., Kumawat, A., Kala, S., & Pal, R. (2022). Soil Erosion and Sediments: A Source of Contamination and Impact on Agriculture Productivity. In *Agrochemicals in Soil and Environment: Impacts and Remediation*. https://doi.org/10.1007/978-981-16-9310-6_14

Renard, K. G., Lane, L. J., Foster, G. R., & Laflen, J. M. (2023). Soil Loss Estimation. In *Soil Erosion, Conservation, and Rehabilitation*. https://doi.org/10.1201/9781003418177-9

Richardson, A. J., & Wiegand, C. L. (1977). Distinguishing vegetation from soil background information.

Photogrammetric Engineering and Remote Sensing, *43*(12).

Salhi, A., Benabdelouahab, S., & Heggy, E. (2024). Growing soil erosion risks and their role in modulating catastrophic floods in North Africa. *International Journal of Applied Earth Observation and Geoinformation*, *133*, 104132.

Sejati, A. W., Waskitaningsih, N., Sukmawati, D. P., Buchori, I., Putri, S. N. A. K., Muzaki, A. J., & Sugiyantoro, Y. (2024). More developed means dangerous: spatial evidence of multi-decadal urbanising watershed and its impact to flash flood in metropolitan Semarang-Indonesia. *Environmental Hazards*, 1–22.

Singh, S., & Kansal, M. L. (2024). A comparative study of morphometric, hydrologic, and semi-empirical methods for the prioritization of sub-watersheds against flash flood-induced landslides in a part of the Indian Himalayan Region. *Environmental Science and Pollution Research*, *31*(41). https://doi.org/10.1007/s11356-023-30613-6

Soniari, N. N., Trigunasih, N. M., Sumarniasih, M. S., & Saifulloh, M. (2024). Exploring soil erodibility: integrating field surveys, laboratory analysis, and geospatial techniques in sloping agricultural terrains. *Journal of Degraded & Mining Lands Management*, *12*(1).

Sugianto, S., Deli, A., Miswar, E., Rusdi, M., & Irham, M. (2022). The Effect of Land Use and Land Cover Changes on Flood Occurrence in Teunom Watershed, Aceh Jaya. *Land*, *11*(8). https://doi.org/10.3390/land11081271

Susila, K. D., Trigunasih, N. M., & Saifulloh, M. (2024). Monitoring Agricultural Drought in Savanna Ecosystems Using the Vegetation Health Index--Implications of Climate Change. *Ecological Engineering & Environmental Technology (EEET)*, *25*(9).

Suyarto, R., Diara, I. W., Susila, K. D., Saifulloh, M., Wiyanti, W., Kusmiyarti, T. B., & Sunarta, I. N. (2023). Landslide inventory mapping derived from multispectral imagery by Support Vector Machine (SVM) algorithm. *IOP Conference Series: Earth and Environmental Science*, *1190*(1). https://doi.org/10.1088/1755-1315/1190/1/012012

Suyarto, R., & Wiyanti. (2023). Studi geomorfologi bentuklahan (landform) skala regional Provinsi Bali. Lembaga Penelitian dan Pengabdian kepada Masyarakat, Universitas Udayana. https://research.unud.ac.id/uploads/penelitian/laporan_akhir/laporan_akhir_penelitian_10865.pdf?655c9490bad81

Taloor, A. K., Khajuria, V., Parsad, G., Bandral, S., Mahajan, S., Singh, S., Sharma, M., & Kothyari, G. C. (2025). Geospatial assessment of soil erosion in the Basantar and Devak watersheds of the NW Himalaya: A study utilizing USLE and RUSLE models. *Geosystems and Geoenvironment*, *4*(2), 100355.

The Guardian. (2025, September 11). Flash floods in Indonesia: Bali deaths. https://www.theguardian.com/world/2025/sep/11/flash-floods-indonesia-bali-deaths

Trigunasih, N. M., Kusmawati, T., & Yuli Lestari, N. W. (2018). Erosion Prediction Analysis and Landuse Planning in Gunggung Watershed, Bali, Indonesia. *IOP Conference Series: Earth and Environmental Science*, *123*(1). https://doi.org/10.1088/1755-1315/123/1/012025

Trigunasih, N. M., Narka, I. W., & Saifulloh, M. (2023). Measurement of Soil Chemical Properties for Mapping Soil Fertility Status. *International Journal of Design and Nature and Ecodynamics*, *18*(6). https://doi.org/10.18280/ijdne.180611

Trigunasih, N. M., & Saifulloh, M. (2022). The Investigating Water Infiltration Conditions Caused by Annual Urban Flooding Using Integrated Remote Sensing and Geographic Information Systems. *Journal of Environmental Management & Tourism*, *13*(5), 1467–1480.

Trigunasih, N. M., & Saifulloh, M. (2023). Investigation of soil erosion in agro-tourism area: guideline for environmental conservation planning. *Geographia Technica*, *18*(1). https://doi.org/10.21163/GT_2023.181.02

Walkley, A., & Black, I. A. (1934). An examination of the degtjareff method for determining soil organic matter, and a proposed modification of the chromic acid titration method. *Soil Science*, *37*(1). https://doi.org/10.1097/00010694-193401000-00003

Wardhani, F. A., Pravitasari, A. E., & Ridwansyah, I. (2022). Flash flood assessment at Upper Cisadane Watershed using land use/land cover and morphometric factors. *IOP Conference Series: Earth and*

Environmental Science, *1109*(1). https://doi.org/10.1088/1755-1315/1109/1/012002

Wayan Sandi Adnyana, I., Rahman As-syakur, A., Wayan Nuarsa, I., Saifulloh, M., & Setiawati, M. D. (2025). Comparing Soil Erosion Rate Predictions Using USLE Method Based on Conventional and Remote Sensing Data Calculations. In *Remotely Sensed Rivers in the Age of Anthropocene* (pp. 357–392). Springer.

Wink Junior, M. V., dos Santos, L. G., Ribeiro, F. G., & da Trindade, C. S. (2024). Natural disasters and poverty: evidence from a flash flood in Brazil. *Environment, Development and Sustainability*, *26*(9). https://doi.org/10.1007/s10668-023-03623-0

Wischmeier, W. H., & Smith, D. D. (1965). Predicting Rainfall-Erosion Losses From Cropland east of the Rocky Mountains: Guide for Selection of Practices for Soil and Water Conservation. *U.S. Department of Agriculture Handbook No.282*, *28*.

Wischmeier, W., & Smith, D. (1978). Predicting rainfall erosion losses: a guide to conservation planning. In *U.S. Department of Agriculture Handbook No. 537*. https://doi.org/10.1029/TR039i002p00285

Wu, Z., Bhattacharya, B., Xie, P., & Zevenbergen, C. (2023). Improving flash flood forecasting using a frequentist approach to identify rainfall thresholds for flash flood occurrence. *Stochastic Environmental Research and Risk Assessment*, *37*(1). https://doi.org/10.1007/s00477-022-02303-1

Zhang, B., Zhang, G., Fang, H., Wu, S., & Li, C. (2024). Risk assessment of flash flood under climate and land use and land cover change in Tianshan Mountains, China. *International Journal of Disaster Risk Reduction*, *115*, 105019.